nances they produce in multipion events at these energies are presumably, then, not unrealistic. At the same time, we have shown that the main features of the reactions studied can be described by extremely simple ideas, and only with experiments with considerably greater statistics could one hope to disentangle the details of the dynamics involved.

ACKNOWLEDGMENTS

The film used at 3.9 GeV/c was generously loaned to us by the Powell-Birge and Goldhaber-Trilling groups at Lawrence Berkeley Laboratory.

The contributions of Dr. Kohya Abe and Jon Jerome on early phases of this experiment are gratefully acknowledged. We are thankful for helpful discussions with Dr. G. Goldhaber and Dr. L. Van Hove. And, of course, none of this work would have been possible without the continued dedicated efforts of many people in the University of Hawaii High-Energy Physics Group, at the Berkeley Bevatron, and at SLAC.

*Work supported in part by the U. S. Atomic Energy Commission under Contract No. AT(04-3)-511.

[1]P. G. Wohlmut *et al.*, Nucl. Phys. B18, 505 (1970).

[2]K. Abe *et al.*, Phys. Rev. D 2, 91 (1970).

[3]Further details on this work can be found in the Ph.D. thesis of A. D. Johnson, University of Hawaii (unpublished). Additional information concerning the 11.9-GeV/c data not directly related to the subject of this paper can be found in the Ph.D. theses of P. G. Wohlmut and A. Yee, University of Hawaii (unpublished).

[4]E. Ferrari and F. Selleri, Nuovo Cimento 21, 1028 (1961).

[5]M. L. Good and W. D. Walker, Phys. Rev. 120, 1857 (1960).

[6]V. J. Stenger, private communication.

[7]G. Ascoli *et al.*, Phys. Rev. Letters 25, 962 (1970).

[8]J. A. Gaidos *et al.*, Phys. Rev. D 2, 1226 (1970).

[9]J. Andrews *et al.*, Phys. Rev. Letters 22, 731 (1969).

[10]J. D. Hansen *et al.*, Nucl. Phys. B25, 605 (1971).

[11]P. G. O. Freund, Phys. Rev. Letters 21, 1375 (1968).

[12]S. U. Chung *et al.*, Phys. Rev. 165, 1491 (1968).

PHYSICAL REVIEW D VOLUME 7, NUMBER 5 1 MARCH 1973

Reaction $pn \to \Delta^{++}(1238)\Delta^{-}(1238)$ at 5.9 GeV/c*

A. R. Kirschbaum and E. Colton

Lawrence Berkeley Laboratory, University of California, Berkeley, California 94720

(Received 30 August 1972)

We present a study of the reaction $pn \to p\pi^+\pi^-n$. The cross section is found to be 4.75 ± 0.25 mb at 5.9 GeV/c. Decay spherical-harmonic moments are presented for peripheral $|T_\ell| = \frac{3}{2}\pi N$ systems as a function of πN-invariant mass. The cross section for the quasi-two-body process $pn \to \Delta^{++}\Delta^{-}$ is found to be 1.90 ± 0.14 mb; the differential cross sections and isobar decays are also studied. The data are not consistent with the predictions of simple one-pion exchange.

I. INTRODUCTION

In this work we present a study of the reaction

$$pn \to \Delta^{++}(1238)\Delta^{-}(1238) \qquad (1.1)$$

at an incident proton momentum of 5.9 GeV/c. Previous analyses of reaction (1.1) have been presented[1,2] at 3.7 and 7.0 GeV/c. Double-Δ(1238) production data have been compared with the one-pion-exchange model and the Białas-Zalewski[3] quark-model predictions in studies of reaction (1.1) as well as in other reactions. In this analysis we simply present the data and compare with previous experimental results.

The reaction (1.1) data are studied in detail in the peripheral region. The possible exotic exchange process with the Δ^{-}(1238) emitted in the forward c.m. hemisphere is not considered here.[4] We present total and differential cross sections for reaction (1.1); in addition, we calculate the joint $\Delta\Delta$ decay density-matrix elements, in order to help expedite any future theoretical studies of decay correlations, etc.

In Sec. II we discuss the experimental separation of the reaction (1.1) data from accepted kinematic fits of the reaction

$$pd \to p_s pn\pi^+\pi^- . \quad (1.2)$$

The invariant-mass dependences and momentum-transfer distributions are illustrated in Sec. III along with the fits to these spectra. The $|T_z| = \frac{3}{2}$ Jackson decay angular distributions are studied as a function of πN invariant mass in Sec. IV. In Sec. V we discuss the decay angular dependences in reaction (1.1). Our conclusions are given in Sec. VI.

II. EXPERIMENTAL DETAILS

The data for reaction (1.2) were obtained in an exposure of the Lawrence Berkeley Laboratory 72-in. liquid-deuterium bubble chamber to a separated 5.9-GeV/c proton beam. Twenty-one rolls of this film were carefully scanned twice for all three-prong events and all four-prong events with at least one stopping positive track. These data, which we refer to as sample A, were measured on the LBL flying spot digitizer (FSD). The measurements were processed through the PANAL-TVGP-SQUAW program system. Kinematic fits were attempted to hypothesis (1.2) as well as the constrained processes

$$pd \to p_s pp\pi^- , \quad (2.1)$$

$$pd \to p_s pp\pi^-\pi^0 , \quad (2.2)$$

$$pd \to pd\pi^+\pi^- . \quad (2.3)$$

In all fits except (2.3), the fitting procedure used the measured value for four-prong events as the starting value for the spectator (p_s) momentum. Three-prong events are those with the spectator protons too slow ($P \leq 80$ MeV/c) to produce an observable track; thus, starting values of 0 ± 30, 0 ± 30, and 0 ± 40 MeV/c were used for P_x, P_y, and P_z, respectively. Fits were accepted only if the inferred projected length of the spectator track was consistent with the observed length.[5] Each passing (confidence level $> 10^{-5}$) kinematic fit was checked for ionization consistency. Events fitting both four-constraint (4C) and one-constraint (1C) hypotheses were assigned to the higher constraint class in all cases. For events fitting several 1C hypotheses, assignment was to the fit with highest kinematic confidence level (CL).

At this point, events assigned to reaction (1.2) sometimes involved a neutron spectator; since we desired events with proton spectators, we required the fitted momentum of the slowest proton to be less than that of the outgoing neutron. Further purification of the surviving reaction (1.2) events was achieved by utilizing only fits with CL > 2%, and by requiring the invariant mass of the $p_s n$ system to be greater than 1.886 GeV. This latter cut removed all residual coherent contamination [i.e., process (2.3)]. Finally, the fitted spectator momentum was required to be less than 0.3 GeV/c in order to minimize the contributions of double scattering. In this way a sample (A) of 2152 events of reaction (1.2) was obtained for further analysis.

The fitted proton spectator momentum distribution for the 612 four-prong events of sample A is displayed in Fig. 1(a); the smooth curve represents the Hulthén distribution[6] normalized to the data in the 90- to 100-MeV/c bin. The laboratory angular distribution of the spectator proton exhibited in Fig. 1(b) is in fair agreement with the shown expected behavior of an isotropic distribution modified by the flux-factor[7] dependence on the initial neutron direction of motion. Of course, distributions corresponding to those in Figs. 1(a) and 1(b) for the 1540 three-prong events cannot be reproduced by the curves in Figs. 1(a) and 1(b). In fact, the fits characteristically yield very small spectator momenta, with outgoing neutrons parallel or antiparallel to the fitted spectator direction. However, all comparisons between the three- and four-prong data of sample A (excluding spectator dependences) indicate a similar behavior. Thus, the 2152 examples of reaction (1.2) can be considered to result from pn collisions, viz.,

$$pn \to pn\pi^+\pi^- . \quad (2.4)$$

The cross section for reaction (2.4) was obtained by normalizing the Hulthén distribution to the four-prong spectator momentum distribution in the 100- to 150-MeV/c region after correcting the data in this region for the various efficiencies, losses, biases, etc. The resulting area under the curve thus yields the total number of reaction (2.4)

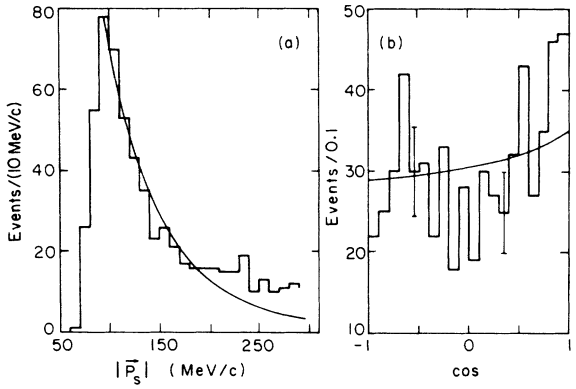

FIG. 1. (a) The fitted spectator momentum distribution for sample A. The curve is the Hulthén distribution normalized to the data in the 90- to 100-MeV/c bin. (b) Laboratory angular distribution of spectator proton. Curve is the expected isotropic behavior modified by the dependence on the initial neutron direction of motion.

events. In this way we obtained a cross section of 4.75 ± 0.25 mb for reaction (2.4) with a 5% Glauber correction.[8]

For the sake of completeness, we also quote here the cross sections for the reactions $pn \to pp\pi^-$ and $pn \to pp\pi^-\pi^0$. They are, respectively, 1.4 ± 0.1 mb and 1.14 ± 0.15 mb.

Another batch of data which we refer to as sample B, is used in parts of the following work when high statistics are necessary. This sample of data, which includes the events of sample A, represents 8008 reaction (2.4) events. The sample B data were selected with no ionization information and with no further CL cuts ($CL > 10^{-5}$ only). In the case of several fits of hypothesis (1.2) for one event, corresponding to an interchange of the π^+ and "fast" proton, we use that fit with the greatest "fast" proton momentum. This procedure experimentally comes closest to effectively creating a fairly pure sample of reaction (2.4) events, especially in the peripheral region.

In the ensuing analyses in this work all three- and four-prong data for reaction (2.4) are combined.

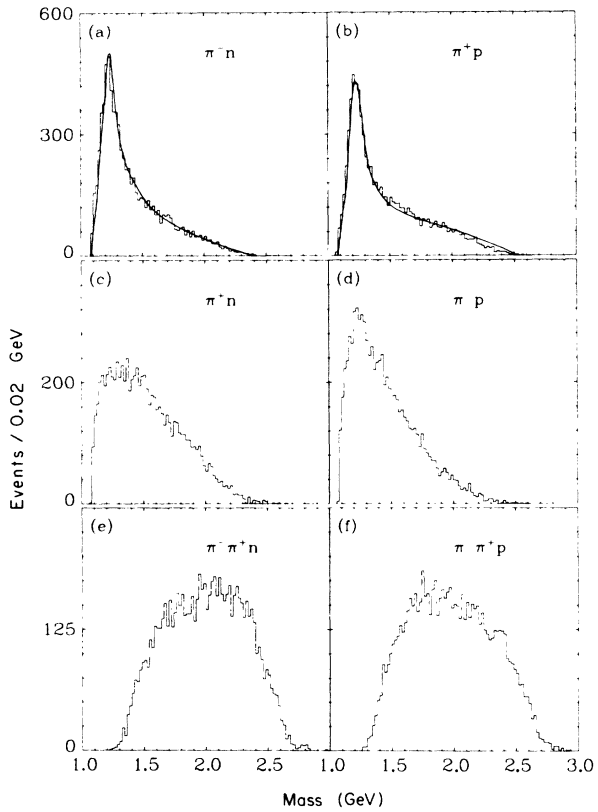

FIG. 2. Two- and three-particle mass distributions (sample B data). Curves are the result of a fit described in text.

III. FITS

Figure 2 displays the four nucleon-pion invariant-mass distributions, as well as the $n\pi^+\pi^-$ and $p\pi^+\pi^-$ distributions, for the events of sample B. It is evident that $\Delta^{++}(1236)$ and $\Delta^-(1236)$ contribute significantly to the final state, and that there are small amounts of $\Delta^0(1236)$ and $\Delta^+(1236)$. A considerable fraction of the final state consists of $\Delta^{++}\Delta^-$ production, as indicated by Fig. 3. To determine the amount of this double-Δ production, we perform a maximum-likelihood fit in which we assume that the final state is a linear combination of the states $p\pi^+\pi^-n$, $\Delta^{++}\pi^-n$, $\Delta^-\pi^+p$, $\Delta^+\pi^-p$, $\Delta^0\pi^+n$, and $\Delta^{++}\Delta^-$. The resonance shape used is one suggested by Jackson[9]

$$F(M) = \frac{M_0\Gamma_0 q_0}{q} \frac{M\Gamma(q)}{(M^2 - M_0^2)^2 + [\Gamma(q)M_0]^2}, \tag{3.1}$$

where q is the decay momentum in the $N\pi$ rest frame, and M is the $N\pi$ invariant mass; M_0 and q_0 are the corresponding central values of these quantities at resonance. The energy dependence of the width is given by[9]

$$\Gamma(q) = \Gamma_0 \left(\frac{q}{q_0}\right)^3 \left(\frac{q_0^2 + m_\pi^2}{q^2 + m_\pi^2}\right). \tag{3.2}$$

In this fit M_0 and Γ_0 were held fixed at the values indicated in Table I, and only the relative amounts were varied. The events used in this fit were those of sample A, for which ionization information was available. It was felt that sample A would afford the most reliable estimate of the resonant fractions. However, sample B has been used in all other parts of this analysis.

Table I shows the results of this fit. The errors are simply the Monte Carlo errors obtained from the error matrix of this fit. The fraction of $\Delta^{++}\Delta^-$ production corresponds to a cross section[10] of

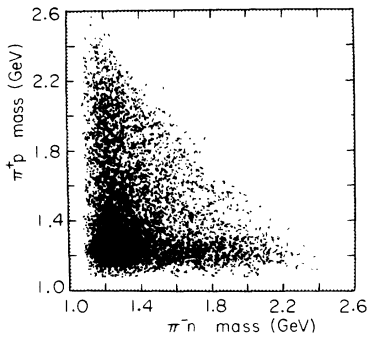

FIG. 3. π^+p mass versus π^-n mass (sample B data).

TABLE I. Results of maximum-likelihood fit of reaction (2.4) as described in text.

(a) Resonance parameters used in maximum-likelihood fit			(b) Amounts determined from maximum-likelihood fit	
	Mass (GeV)	Width (GeV)	State	Amount (%)
Δ^{++}	1.236	0.120	Nonres.	9.0 ± 2.1
Δ^{+}	1.236	0.120	$\Delta^{++}\pi^{-}n$	8.2 ± 1.5
Δ^{-}	1.240	0.150	$\Delta^{+}\pi^{-}p$	9.0 ± 1.1
Δ^{0}	1.236	0.120	$\Delta^{-}\pi^{-}p$	14.3 ± 1.7
			$\Delta^{0}\pi^{+}n$	19.4 ± 1.3
			$\Delta^{++}\Delta^{-}$	40.1 ± 1.6

1.90 ± 0.14 mb for the process $pn \to \Delta^{++}\Delta^{-}$. Shapira *et al.*[2] find that the cross sections $\sigma(\bar{p}p \to \bar{\Delta}^{--}\Delta^{++})$, $\sigma(pn \to \Delta^{++}\Delta^{-})$, and $\frac{9}{2}\sigma(pp \to \Delta^{++}\Delta^{0})$, when plotted against the incident momentum P_L, behave like $P_L^{-2.5}$. Our cross section for $\Delta^{++}\Delta^{-}$ production is consistent with these results. The $\pi^{+}p$ and $\pi^{-}n$ invariant-mass distributions as calculated from our fit have been plotted against the real $\pi^{+}p$ and $\pi^{-}n$ mass distributions (sample B) in Figs. 2(a) and 2(b), respectively, the curves having been normalized to the total number of events. As expected, the agreement is good.

Following Shapira *et al.*,[2] we adopt the criterion

$$F(M_{\pi^{+}p})F(M_{\pi^{-}n}) > 0.2 \tag{3.3}$$

for selecting the cleanest possible sample of $\Delta^{++}\Delta^{-}$ events. In addition, we restrict the analysis to events in which the Δ^{++} is produced in the forward c.m. hemisphere. This sample contains 955 events and will be used in our subsequent analysis of $\Delta^{++}\Delta^{-}$ production and decay in Sec. V, as well as in our fits to the differential cross sections described below.

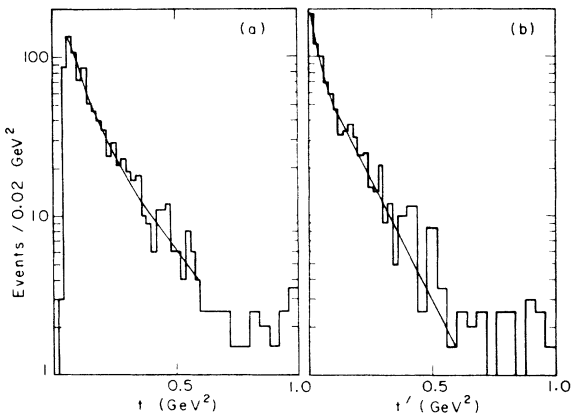

FIG. 4. The differential cross sections (a) $d\sigma/dt$ and (b) $d\sigma/dt'$ for $\Delta^{++}\Delta^{-}$ events. The curves are the results of least-squares fits described in the text.

In Figs. 4(a) and 4(b) we plot the differential cross sections $d\sigma/dt$ and $d\sigma/dt'$, respectively, for $\Delta^{++}\Delta^{-}$ events, where $t' = t - t_{\min}$. The $d\sigma/dt$ distribution for $0.06 < t < 0.6$ GeV^2 was fitted to the assumed form

$$N = Ae^{-at} + Be^{-bt} \tag{3.4}$$

by using a least-squares technique. A fit to $d\sigma/dt'$ for $t' < 0.6$ GeV^2 was performed by using the same functional form. The results of these fits are listed in Table II. The smooth curves drawn in Fig. 4 represent Eq. (3.4), using the best-fit values of the free parameters.

IV. $|T_z| = \frac{3}{2}$ DECAY ANGULAR DISTRIBUTIONS

In this section we study the scattering angular distributions in the $|T_z| = \frac{3}{2}$ πN rest systems for low momentum transfer from the incoming proton to the outgoing $\pi^{+}p$ system.[11] Using the method of moments, we calculate $\langle Y_L^M \rangle$ and display them as a function of πN invariant mass for $t < 0.5$ GeV^2. We take

$$\langle Y_L^M \rangle = \frac{1}{N}\sum_{i=1}^{N} Y_L^M(\theta_i, \phi_i), \tag{4.1}$$

TABLE II. Fit of t and t' distributions for $\Delta^{++}\Delta^{-}$ events to the assumed form $N = Ae^{-at} + Be^{-bt}$.

Quantity	t distribution	t' distribution
t (t') range (GeV^2)	0.06–0.60	0–0.60
χ^2	18.1	39.8
No. points	27	30
A	269 ± 64	139 ± 26
B	65 ± 25	100 ± 13
a (GeV^{-2})	−16.3 ± 4.8	−39.2 ± 11.7
b (GeV^{-2})	−4.6 ± 0.8	−7.0 ± 0.5

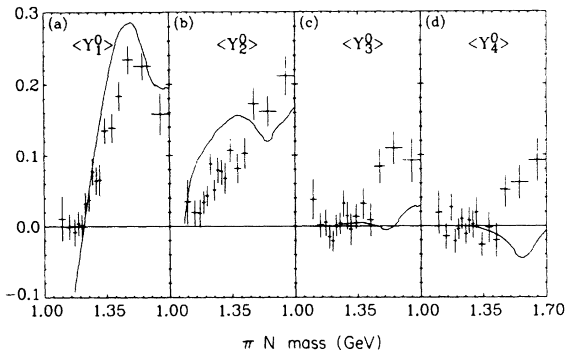

FIG. 5. The moments $\langle Y_L^0\rangle$, $L = 1-4$, for events with $t < 0.5$ GeV^2. The π^+p and π^-n data are combined.

where θ and ϕ are the polar and azimuthal angles, respectively, of the outgoing nucleon in the standard t-channel coordinate system.[12] Corresponding data for both π^+p and π^-n systems are similar; thus, they are combined in this section. Since large statistics are required we use the sample B data.

In Figs. 5(a)–5(d) we display the combined $L = 1-4$ $\langle Y_L^0\rangle$ moments. The smooth curves represent known π^+p elastic scattering angular distributions; the curves were drawn through points calculated from the CERN phase shifts.[13] In fact, these curves just represent unadorned one-pion-exchange-model predictions for the $pn \to (p\pi^+)(\pi^-n)$ data. Clearly, other considerations are necessary.[14] In Fig. 6 we show the nonzero-M $\langle \mathrm{Re}\,Y_L^M\rangle$ and $\langle \mathrm{Im}\,Y_L^M\rangle$ moments for L values of 1 and 2. The

TABLE III. Joint decay distribution for $pn \to \Delta^{++}\Delta^-$. Barred angles refer to Δ^{++}. For explanation of other symbols, see Ref. 16.[a]

Term	a_i	f_i
1	$\rho^{33}-\rho^{11}$	$\frac{5}{4}\langle 1-3\cos^2\bar\theta\rangle$
2	$\mathrm{Re}\,\rho^{31}$	$-\frac{5}{8}\sqrt{3}\,\langle\sin 2\bar\theta\cos\bar\phi\rangle$
3	$\mathrm{Re}\,\rho^{3\,-1}$	$-\frac{5}{8}\sqrt{3}\,\langle\sin^2\bar\theta\cos 2\bar\phi\rangle$
4	$\rho_{33}-\rho_{11}$	$\frac{5}{4}\langle 1-3\cos^2\theta\rangle$
5	$\mathrm{Re}\,\rho_{31}$	$-\frac{5}{8}\sqrt{3}\,\langle\sin 2\theta\cos\phi\rangle$
6	$\mathrm{Re}\,\rho_{3\,-1}$	$-\frac{5}{8}\sqrt{3}\,\langle\sin^2\theta\cos 2\phi\rangle$
7	$\rho^{33}_{-}-\rho^{11}_{-}$	$\frac{50}{16}\langle(1-3\cos^2\theta)(1-3\cos^2\bar\theta)\rangle$
8	$\mathrm{Re}\,\rho^{31}_{-}$	$-\frac{25}{16}\sqrt{3}\,\langle(1-3\cos^2\theta)\sin 2\bar\theta\cos\bar\phi\rangle$
9	$\mathrm{Re}\,\rho^{3\,-1}_{-}$	$-\frac{25}{16}\sqrt{3}\,\langle(\sin^2\bar\theta\cos 2\bar\phi)(1-3\cos^2\theta)\rangle$
10	$\mathrm{Re}\,\rho^{-}_{31}$	$-\frac{25}{16}\sqrt{3}\,\langle(1-3\cos^2\bar\theta)\sin 2\theta\cos\phi\rangle$
11	$\mathrm{Re}\,\rho^{-}_{3\,-1}$	$-\frac{25}{16}\sqrt{3}\,\langle(\sin^2\theta\cos 2\phi)(1-3\cos^2\bar\theta)\rangle$
12	$\mathrm{Re}\,(\rho^{31}_{31}-\rho^{-1\,-3}_{31})$	$\frac{225}{96}\langle\sin 2\theta\sin 2\bar\theta\cos(\phi+\bar\phi)\rangle$
13	$\mathrm{Re}\,(\rho^{31}_{13}-\rho^{-1\,-3}_{13})$	$\frac{225}{96}\langle\sin 2\theta\sin 2\bar\theta\cos(\phi-\bar\phi)\rangle$
14	$\mathrm{Re}\,(\rho^{3\,-1}_{31}+\rho^{1\,-3}_{31})$	$\frac{225}{96}\langle\sin 2\theta\sin^2\bar\theta\cos(2\bar\phi+\phi)\rangle$
15	$\mathrm{Re}\,(\rho^{3\,-1}_{13}+\rho^{1\,-3}_{13})$	$\frac{225}{96}\langle\sin 2\theta\sin^2\bar\theta\cos(2\bar\phi-\phi)\rangle$
16	$\mathrm{Re}\,(\rho^{31}_{3\,-1}-\rho^{-1\,-3}_{3\,-1})$	$\frac{225}{96}\langle\sin 2\bar\theta\sin^2\theta\cos(2\phi+\bar\phi)\rangle$
17	$\mathrm{Re}\,(\rho^{31}_{-13}-\rho^{-1\,-3}_{-13})$	$\frac{225}{96}\langle\sin 2\bar\theta\sin^2\theta\cos(2\phi-\bar\phi)\rangle$
18	$\mathrm{Re}\,(\rho^{3\,-1}_{3\,-1}+\rho^{1\,-3}_{3\,-1})$	$\frac{75}{32}\langle\sin^2\bar\theta\sin^2\theta\cos 2(\phi+\bar\phi)\rangle$
19	$\mathrm{Re}\,(\rho^{3\,-1}_{-13}+\rho^{1\,-3}_{-13})$	$-\frac{25}{16}\sqrt{3}\,\langle\sin^2\bar\theta\cos 2\bar\phi\,(1-3\cos^2\theta)\rangle$

[a] Here $\rho^{-}_{nn'}=\rho^{11}_{nn'}+\rho^{-1\,-1}_{nn'}-2\rho^{00}_{nn'}$, and $\rho^{mm'}_{-}=\rho^{mm'}_{33}+\rho^{mm'}_{-3-3}-\rho^{mm'}_{11}-\rho^{mm'}_{-1-1}$.

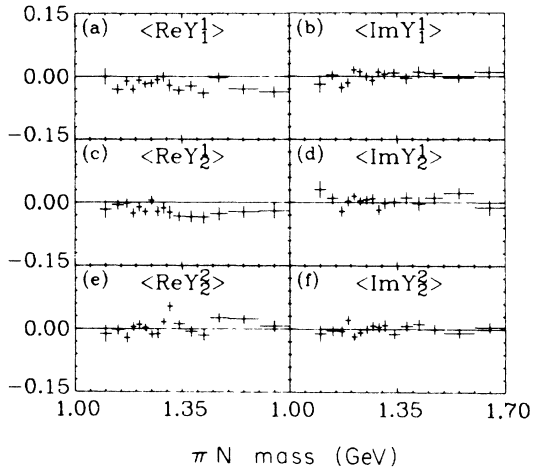

FIG. 6. The moments $\langle Y_L^M \rangle$, $M \neq 0$, $L = 1, 2$ for events with $t < 0.5$ GeV^2. The $\pi^+ p$ and $\pi^- n$ data are combined.

$\langle \mathrm{Im} Y_L^M \rangle$ are consistent with zero as required by parity conservation.[15] The $\langle \mathrm{Re} Y_L^1 \rangle$ average near -0.03 over the entire range of πN mass. This result is also inconsistent with unmodified one-pion-exchange-model predictions (zero).

V. $\Delta^{++}\Delta^{-}$ DECAY CORRELATIONS

To study the decay correlations for $\Delta^{++}\Delta^{-}$, we adopt the formalism of Pilkuhn and Svensson,[16] as used by Shapira *et al.*[2] and Borecka *et al.*[17] We write the joint decay distribution as

$$16\pi^2 W(\Omega_1, \Omega_2) = 1 + \sum_{i=1}^{19} a_i f_i(\Omega_1, \Omega_2), \qquad (5.1)$$

where the functions f_i are orthogonal functions of the solid angles Ω_1 and Ω_2, which are, respectively, the t-channel[12] Δ^{++} and Δ^{-} decay angles as seen in the Δ^{++} and Δ^{-} rest frames. The coefficients

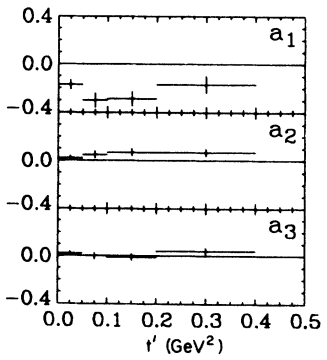

FIG. 7. Single isobar moments for $\Delta^{++}\Delta^{-}$ events. The following moments have been averaged and plotted together: a_1 and a_4, a_2 and a_5, a_3 and a_6.

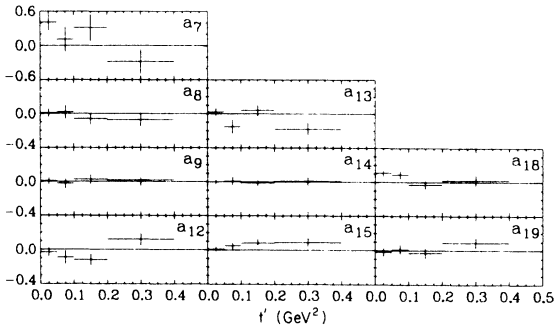

FIG. 8. Double isobar moments for $\Delta^{++}\Delta^{-}$ events. The following moments have been averaged and plotted together: a_8 and a_{10}, a_9 and a_{11}, a_{14} and a_{16}, a_{15} and $-a_{17}$.

a_i are written in terms of the joint density-matrix elements. Table III lists both the coefficients a_i and the functions f_i. The first 6 of these 19 terms specify the decay angular distributions of the single isobars, as can be seen by integrating Eq. (5.1) over first Ω_1 and then Ω_2. The remaining 13 terms describe the correlations between the decays of both isobars.

For reaction (1.1), there are in fact only 12 independent coefficients. Charge independence requires that the following coefficients must be pairwise equal: a_1 and a_4, a_2 and a_5, a_3 and a_6, a_8 and a_{10}, a_9 and a_{11}, a_{14} and a_{16}, and a_{15} and $-a_{17}$.

We have evaluated all 19 coefficients a_i, using the method of moments for four bins in t' over the range $0 < t' < 0.4$ GeV^2. Since the coefficients predicted to be equal are in fact so within errors, these pairs of coefficients were averaged and plotted along with the remaining a_i in Figs. 7 and 8. Simple one-pion exchange predicts that $a_1 = a_4 = -\frac{1}{2}$ and $a_7 = \frac{1}{2}$, with all other a_i equal to zero. In fact, a_1 and a_4 are significantly different from the predicted value throughout the range $0 < t' < 0.4$ GeV^2, and a_{18} is nonzero at small t'. The remaining a_i are consistent with the predictions, at least for small t'.

The single-isobar moments of Fig. 7 may be compared with those found by Shapira *et al.*[2] for reaction (1.1) at 7 GeV/c. The agreement is generally good. They present the double-isobar moments in a different fashion than we do, and direct comparison is not feasible. However, Borecka *et al.*[17] present plots of the 12 independent moments for the reaction $\bar{p}p \to \bar{\Delta}^{--}\Delta^{++}$ at 12 GeV/c, and they are consistent with the moments shown in Figs. 7 and 8.

In Fig. 9 we plot the single-particle decay distributions $\cos\theta$ and ϕ for $\Delta^{++}\Delta^{-}$ events having t' < 0.4 GeV^2, where the corresponding distributions

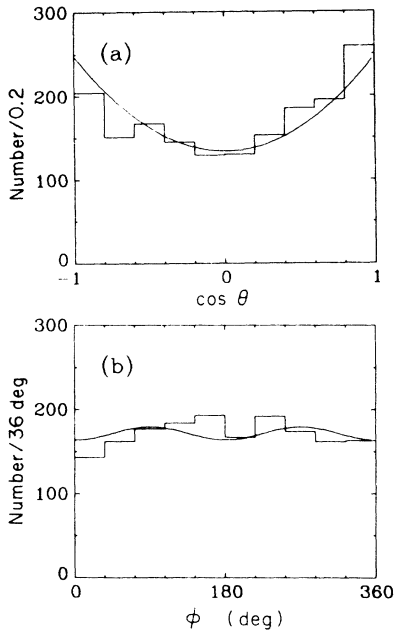

FIG. 9. The Jackson angles (a) $\cos\theta$ and (b) ϕ for $\Delta^{++}\Delta^{-}$ events having $t' < 0.4$ GeV^2. The corresponding distributions for Δ^{++} and Δ^{-} are combined.

for each isobar are plotted together. The curves are, respectively, $W(\cos\theta_1)+W(\cos\theta_2)$ and $W(\phi_1)+W(\phi_2)$ normalized to the total number of events, where

$$W(\cos\theta) = \tfrac{1}{2}[1-(\rho_{33}-\rho_{11})(3\cos^2\theta-1)],$$
$$W(\phi) = \frac{1}{2\pi}\left[1-\frac{4}{\sqrt{3}}(\mathrm{Re}\rho^{3\,-1}\cos 2\phi)\right]. \tag{5.2}$$

Equations (5.2), which represent the decay of a pure spin-$\frac{3}{2}$ particle, were obtained by integrating Eq. (5.1). The density-matrix elements in Eqs. (5.2) were obtained by averaging the results of Fig. 5 over the range $0 < t' < 0.4$ GeV^2.

VI. CONCLUSION

We have presented data on the reaction $pn \to p\pi^+\pi^-n$, and in particular on the subsample of events consisting of $\Delta^{++}\Delta^{-}$ production. The total cross section and differential cross section $d\sigma/dt'$ are consistent with results of other workers. The decay spherical harmonic moments are seen to be incompatible with simple one-pion exchange. We have also analyzed the joint decay properties of the $\Delta^{++}\Delta^{-}$ system and have presented the results in terms of the joint density-matrix elements, which are consistent with those found by other workers.

ACKNOWLEDGMENTS

We thank W. Gage and Professor W. Chinowsky for assistance during the early stages of this experiment. We also thank the crew of the 72-in. bubble chamber.

---

*Work done under the auspices of the U. S. Atomic Energy Commission.

[1] H. O. Cohn, R. D. McCulloch, W. M. Bugg, and G.T. Condo, Phys. Letters 26B, 598 (1968).

[2] A. Shapira *et al.*, Nucl. Phys. B23, 583 (1970).

[3] A. Bialas and K. Zalewski, Nucl. Phys. B6, 465 (1968).

[4] For an analysis of this process at 7 GeV/c see, e.g., G. Yekutieli *et al.*, Phys. Rev. Letters 25, 184 (1970).

[5] In practice this meant a tolerance of ± 1.0 mm inconsistency between the "fitted" length and the observed length. Momentum uncertainties were great enough to absorb such variations without significantly affecting the χ^2 of the fit.

[6] L. Hulthén and M. Sugawara, in *Handbuch der Physik*, edited by S. Flügge (Springer, Berlin, Germany, 1957), Vol. 39, Chap. 1.

[7] See, e.g., R. G. Newton, *Scattering Theory of Waves and Particles* (McGraw-Hill, New York, 1966), Chap. 8.

[8] This correction is due to a loss of events where the neutron is screened by the proton in the deuteron. See, e.g., R. Glauber, Phys. Rev. 100, 242 (1955).

[9] J. D. Jackson, Nuovo Cimento 34, 1644 (1964).

[10] The error in this cross section is obtained by adding in quadrature the fitted error in the amount of $\Delta^{++}\Delta^{-}$ and the experimental cross-section error for $pn \to pn\pi^+\pi^-$.

[11] T_z represents the z component of isotopic spin.

[12] In the t-channel coordinate system, the appropriate incoming nucleon as seen in the πN rest frame is the polar or z axis, and the y axis is along the normal to the production plane.

[13] A. Donnachie, R. G. Kirsopp, and C. Lovelace, CERN Report No. CERN-TH-838, Addendum, 1967 (unpublished).

[14] For a discussion of some other contributions see, e.g., E. Colton and A. R. Kirschbaum, Phys. Rev. D 6, 95 (1972).

[15] This is true if the y axis is taken to be the normal to the production plane.

[16] H. Pilkuhn and B. E. Y. Svensson, Nuovo Cimento 38, 518 (1965).

[17] L. Borecka *et al.*, Nuovo Cimento 5A, 19 (1971).